PEM/AEM Junction Design for Bipolar Membrane Fuel Cells

John M. Ahlfield,[a,*] Lisha Liu,[b,*] and Paul A. Kohl[a,,z]**

[a]*School of Chemical and Biomolecular Engineering, Georgia Institute of Technology, Atlanta, Georgia 30332, USA*
[b]*School of Materials Science and Engineering, Georgia Institute of Technology, Atlanta, Georgia 30332, USA*

The combination of proton exchange membrane (PEM) and anion exchange membrane (AEM) materials to form a bipolar membrane (BPM) is of interest in hybrid electrochemical devices to mitigate the disadvantages of their monopolar counterparts. The PEM-AEM interface is a critical component in bipolar membrane fuel cell operation. In this study, mono- and di-membrane bipolar membranes were fabricated. Interfacial materials with varying conductivities were used in order to control the location of the junction within the di-membrane BPMs. Mono-membrane BPMs were constructed via conversion of a single face of a monopolar membrane (Nafion). The membranes were used in fully functional fuel cells and characterized via electrochemical impedance spectroscopy (EIS). For the di-membrane BPMs, use of a conductive interface consisting of a single ion conductive material resulted in devices with lower interfacial resistance as compared to a neutral interface. When comparing conductive interface materials, anion-conductive materials provided lower total membrane resistance than proton-conductive materials. This decrease is due to positioning the junction closer to the anode and farther from the air-cathode. These results show that the formation of the optimal junction is critically dependent on fabrication technique and location.

Manuscript submitted May 19, 2017; revised manuscript received August 10, 2017. Published August 24, 2017. This was Paper 2528 presented at the Honolulu, Hawaii, Meeting of the Society, October 2–7, 2016.

Polymeric membrane-based fuel cells are a promising candidate to provide clean, efficient, and energy dense power sources. Of the primary types of these fuel cells, proton exchange membrane (PEM) fuel cells have capabilities of producing extremely high power densities, and the materials used as the proton exchange membrane (e.g. Nafion) are thermally and mechanically robust, allowing for long-term operation. Despite these features, there are several drawbacks relating to the operation of these devices under acidic conditions. First, the migration of protons from anode to cathode results in electro-osmotic drag of water (and methanol, where applicable) which can lead to a phenomenon known as "cathode flooding" or a blockage of transport passageways with water. Second, both the catalytic and polymeric materials required to survive the harsh acidic operating environment are expensive to manufacture. Third, both the metal catalyst and its carbon support are subject to corrosion at low pH.

One alternative to the PEM fuel cell is the anion exchange membrane (AEM) fuel cell. This configuration addresses many of the shortcomings of the PEM cell simply by operating under alkaline (high pH) conditions. AEM fuel cells potentially address many of the issues inherent with PEM devices. The basic operating environment is much more conducive to the oxygen reduction reaction (ORR), which opens the possibility of using non-platinum based (cheaper) catalysts.[1–3] Additionally, anion exchange membranes are typically hydrocarbon based, and as such are less expensive to manufacture than Nafion and other perfluorosulfonic acid (PFSA) membranes used in PEM devices. Another benefit is the reversed direction of ion transport through the membrane, which opposes fuel crossover rather than supplementing it.[2,3] This could lead to the use of more pure liquid fuels (such as methanol) in AEM devices. Unfortunately, AEM fuel cells are limited by the anion exchange materials themselves. Currently, there are no anion exchange membranes widely available on the market with ionic conductivities rivalling Nafion. Additionally, AEMs are not as mechanically or chemically robust as their PEM counterparts.

A newer development, bipolar (or hybrid) fuel cells (Figure 1) are an attempt to combine the established PEM architecture with the advantages potentially offered by AEMs.[4] The bipolar name comes from the opposing polarity at the electrodes – one electrode is operated at low pH while the other operates at high pH. The bipolar device offers a few distinct advantages compared to fully acidic or alkaline fuel cells. It allows for the study and evaluation of AEM ionomers separately from anion exchange membranes, which has resulted in a few materials being developed explicitly as ionomers rather than membranes.[5] Because ionomers and membranes serve different functions in the cell, it is reasonable to assume that the materials used for these functions should be different. However, in order to study AEM ionomers previously, they were required to be used in conjunction with an anion exchange membrane, which makes deconvolution of ionomer from membrane performance difficult.

A recent publication by Grew[6] provides a computational guideline for transport at the critical PEM/AEM junction in BPM-based devices. In this work, it is shown that for a device with acidic anode and alkaline cathode (Figure 1b), the recombination rate of the proton/hydroxyl groups at the interface is the limiting component for device performance. Additionally, the recombination rate can be increased by having a concentration gradient of the ions in the recombination region, rather than an abrupt junction of the two opposing polarity regions.

In the initial work on these devices, the bipolar membranes were formed by pressing the half cells (PEM and AEM) using a diluted solution of Nafion ionomer suspension to bind the membranes together.[4,7] In this study, only devices with the acidic anode/alkaline cathode (Figure 1b) will be considered. The material used in the interfacial region will be varied in order to understand the effect of PEM/AEM junction location on the overall performance of the cell. Each junction material provides a different location for the recombination of ions in the device: i) on the surface of the AEM, ii) on the surface of the PEM, or iii) anywhere in the dilute junction region of the cell. Fabrication of a mono-membrane BPM via Nafion conversion is also explored here.

Experimental

Materials.—The membranes used in this study were Nafion 117 and Tokuyama A-201. The Nafion was pre-treated by sequential boiling steps in 3% H_2O_2, H_2O, 1M H_2SO_4, and again in H_2O. Each boil lasted approximately 1 hour. All membranes were stored in distilled water until MEA fabrication. A 5% Nafion dispersion in alcohol and a 5% Tokuyama AS-4 solution were used as the PEM and AEM ionomers, respectively. All other chemicals were used as received.

Junction material preparation for Di-membrane BPMs.—Three different interfacial materials were prepared for this study: i) a neutral layer containing epoxy, ii) a proton conductive layer, and iii) an anion conductive layer. Direct contact of two pieces of AS-4 did not result in a usable interface because of the lack of adhesion. To

*Electrochemical Society Student Member.
**Electrochemical Society Fellow.
[z]E-mail: kohl@gatech.edu

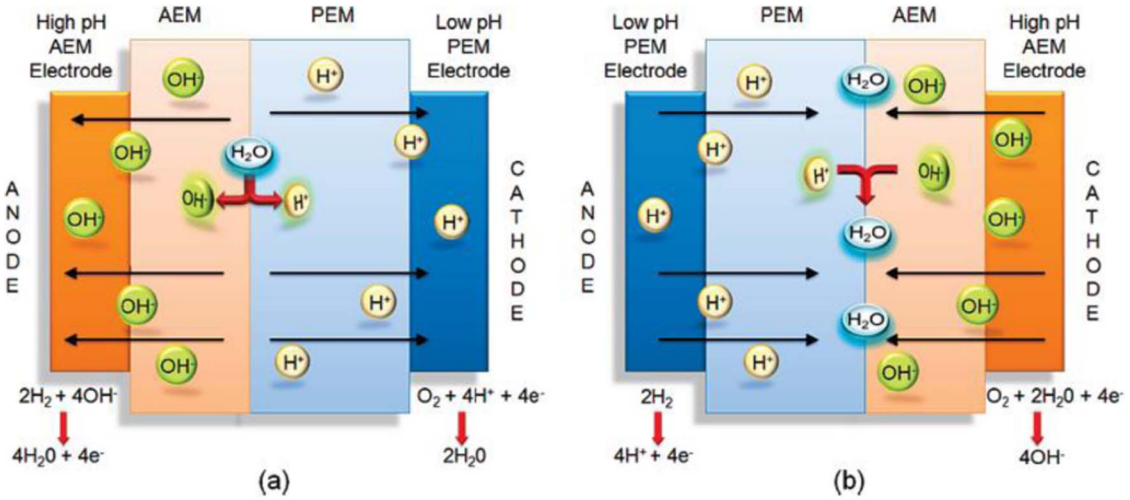

Figure 1. Anode (a) and cathode (b) hybrid fuel cells.

prepare the neutral interface, a small amount of dried Nafion was produced by evaporating the solvent from the Nafion dispersion. An equal mass of an anion conductive polymer and dried Nafion was dissolved in dimethylacetamide (DMAc). Trimethylolpropane trigylcidyl ether (TMPTGE) was added to the solution containing the PEM/AEM ionomers, corresponding to 4% by weight relative to the solid ionomer content (i.e. 4 mg epoxy for every 100 mg of total ionomer mass). The final mixture of the PEM/AEM ionomers and TMPTGE was used as the neutral interface. To prepare the proton conductive interface, 5% Nafion dispersion was used as-received. To prepare the anion conductive interface, a hydroxide-containing ionic liquid (1-butyl-3-methylimidazolium hydroxide, [bmim][OH]) was synthesized from [bmim][Cl]. Due to the high viscosity of the ionic liquid at room temperature, THF was used to dilute the [bmim][OH] to 10% v/v. The structure of these materials is shown in Figure 2.

Conversion of Nafion into mono-membrane BPM.—The conversion of Nafion's proton conductive sulfonic acid head groups to anion conductive quaternary ammonium groups was carried out over 3

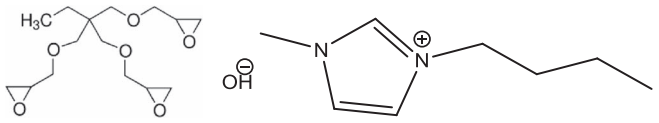

Figure 2. TMPTGE (left) and [bmim][OH] (right).

reactions, shown in Scheme 1. For each reaction, a flask was charged with the desired reagent, then the Nafion membrane was stretched over the flask opening and held down with elastic rings. By inverting this assembly onto a Petri dish at the desired temperature, reacting only a single face of the film could be ensured. The film was first reacted with thionyl chloride at 80°C for 12 hours. The resulting sulfonyl chloride form was then introduced to a large excess of N,N-Dimethyl-1,3-diaminopropane for 12 hours at 50°C to form a sulfonamide structure. Finally, the sulfonamide was reacted with an excess of methyl iodide overnight at room temperature to form the quaternary ammonium salt. After each step, the film was boiled in H_2O for 3 hours followed by

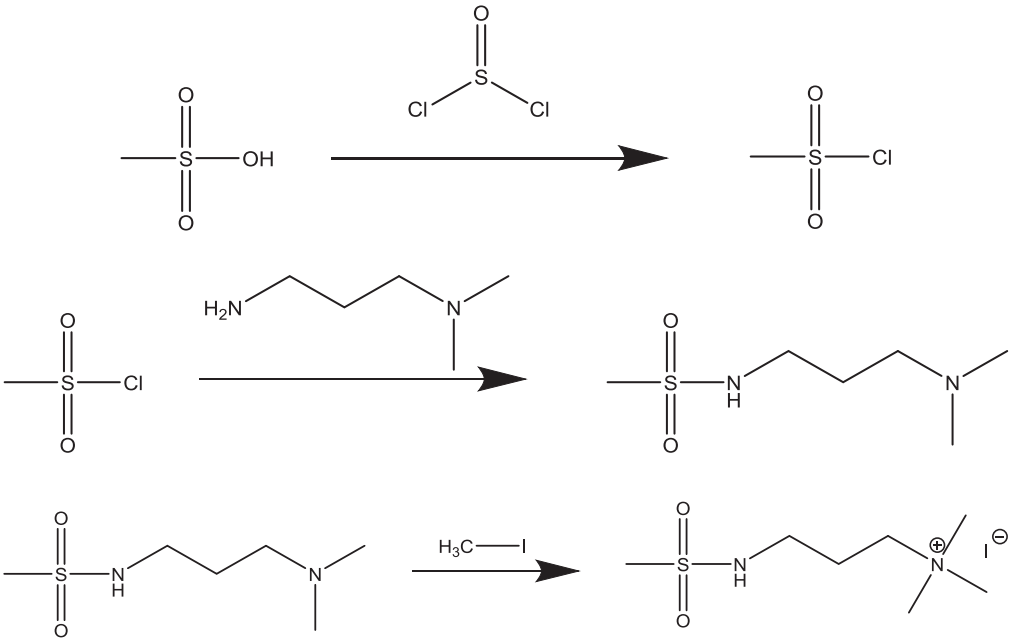

Scheme 1. Conversion of sulfonic acid head groups to a quaternary ammonium moiety.

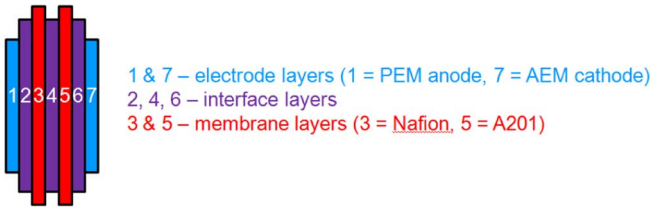

Figure 3. Schematic of MEA layers in the bipolar device.

drying overnight in a vacuum chamber at room temperature, in order to remove any excess reagent trapped in the membrane.

Mono-membrane BPM characterization.—The conversion of Nafion's sulfonic acid groups into quaternary ammonium groups was determined using a combination of X-ray photoelectron spectroscopy (XPS) and secondary ion mass spectroscopy (SIMS). The XPS data was used to calculate the conversion at the film's surface, followed by depth profiling using SIMS in order to determine the penetration depth of the conversion. The XPS was performed on a Thermo Scientific K-Alpha XPS, while the SIMS was performed using an IONTOF 5–300 Time-of-Flight SIMS.

Electrode fabrication.—The PEM anode and AEM cathode were both fabricated via slurry method. The PEM anode slurry consisted of Pt/Ru alloy catalyst (75% metal weight – 50% Pt, 25% Ru, 25% C), Nafion dispersion (15% by weight with respect to the catalyst), and a mixture of water/isopropanol. The slurry was sprayed onto hydrophilic Toray 2050 L carbon paper and dried at room temperature. The target metal loading was 4 mg/cm^2 for this low pH electrode. The AEM cathode slurry contained a Pt/C catalyst (40% metal weight), Tokuyama AS-4 ionomer (10% weight with respect to catalyst), and isopropanol. The slurry was sprayed onto hydrophobic Toray TGPH-090 carbon paper and dried at room temperature. The target metal loading for the high pH electrodes was 2 mg/cm^2. After drying, the electrodes were soaked in 0.1 M NaOH overnight to exchange completely to OH^- form. Finally, the electrodes were rinsed in distilled water to remove any excess OH^- ions from the surface. The geometric surface area of the electrodes was 2 cm^2.

Membrane electrode assembly (MEA) preparation.—50 μL of the respective ionomer was sprayed directly onto each electrode surface prior to assembly. Each electrode was then placed directly atop its respective membrane – the acidic anode onto Nafion and the alkaline cathode onto Tokuyama A201. For the di-membrane BPMs, 50 μL of the prepared interfacial material was sprayed onto the face of Nafion to be assembled against the AEM. A representation of the layers is shown in Figure 3. The entire MEA was hot-pressed for 10 minutes at 2 MPa and 60°C. The MEA was placed into a BioLogic Fuel Cell Test Station FCT 150S. Humidified oxygen and hydrogen were fed at 55°C to the cathode and anode at 25 and 10 sccm respectively.

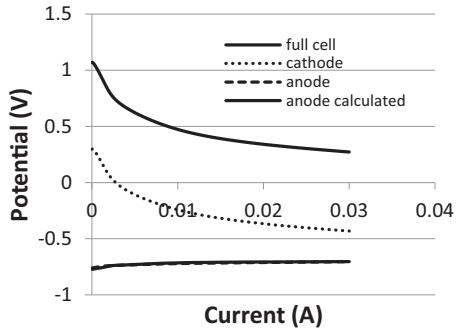

Figure 4. Voltammogram for the neutral junction BPM device (100% RH) showing individual electrodes.

Electrochemical measurements were obtained using a Princeton PAR 2273 potentiostat/galvanostat.

Results and Discussion

Di-membrane BPM MEA testing.—The di-membrane BPMs with different interfacial materials were each tested in otherwise identical MEAs under identical operating conditions. The primary electrochemical measurements carried out were forward/reverse linear voltage sweeps and electrochemical impedance spectroscopy (EIS). The EIS measurements were conducted from 50 mHz to 89 kHz at 300 and 600 mV immediately succeeding a linear sweep.

The first of the di-membrane BPM fuel cells examined was the neutral junction containing both epoxy and PEM/AEM ionomers. The TMPTGE epoxy was used to assist in preventing delamination. Using a reference electrode inserted between the films, each half of the cell's behavior could be isolated. The reference electrode used was a thin Pt wire inserted between the films before hot pressing the MEA. The voltammogram in Figure 4 shows that the anodic (PEM) half cell remains at relatively constant potential over the current range examined, while the cathodic (AEM) half cell behavior drives the full cell potential.

The neutral junction cell was also subjected to humidity variation in order to determine the water management within the device. The three humidity conditions tested were: i) both gas feeds fully humidified (voltammogram shown in Figure 4), ii) dry anodic feed + humidified cathodic feed, and iii) humidified anodic feed + dry cathodic feed. The voltammograms for the three conditions looked nearly identical (Figure 5), prompting further probing to determine what, if any, differences existed between the cells under these humidification conditions.

Electrochemical impedance spectroscopy (EIS) analysis was used in order to differentiate the humidification effect. For these devices, each electrode was modeled as a parallel resistor/capacitor, and the membranes and junction were included as a single series resistor for ease of impedance modeling (Figure 6). The Nyquist plots, Figure 7,

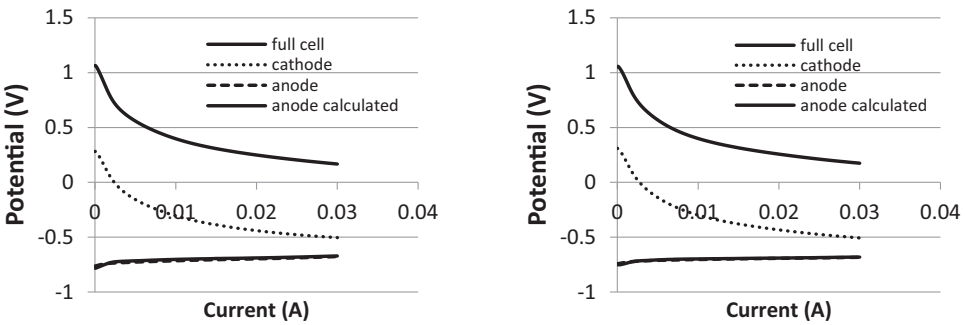

Figure 5. Voltammograms for the neutral junction BPM under humidified cathode/dry anode (left) and humidified anode/dry cathode (right) conditions.

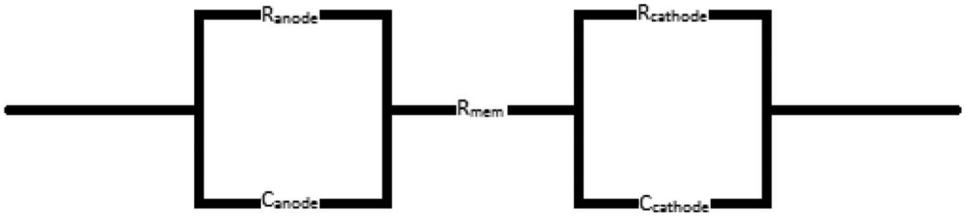

Figure 6. Equivalent circuit used for EIS analysis.

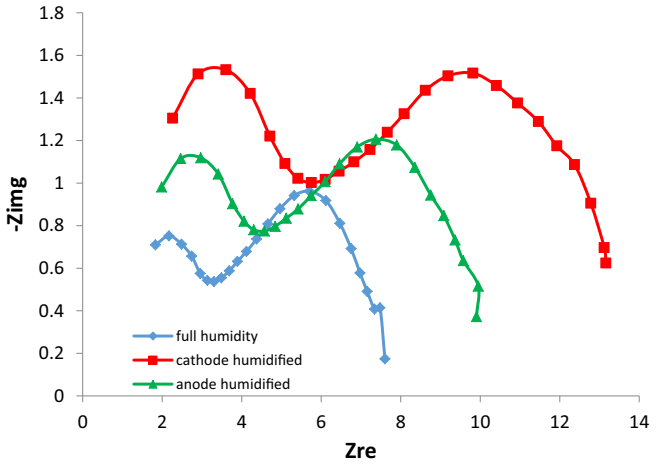

Figure 7. Nyquist plots for neutral junction BPM under varying humidification.

Table I. Computed circuit elements under varying humidification.

Element	100% RH	Cathode humidified	Anode humidified
R_{mem} Ω cm^2	4.8	5.8	5.0
$R_{a,\,ct}$ Ω cm^2	3.6	7.8	5.8
$R_{c,ct}$ Ω cm^2	5.8	10.2	7.8

for these devices at 300 mV (∼28 mA) show a pair of semicircular loops (each corresponding to an electrode) and a translation along the real axis corresponding to the series resistance from the membranes and junction. The low- and high-frequency loops are attributed to the cathode and anode respectively.[8] The extrapolated high frequency intercept is used to determine the membrane and interfacial resistance. The computed circuit elements are tabulated in Table I.

The Nyquist plot shows that the device with both feeds humidified produced the least interfacial resistance (shown by R_{mem}) in addition to having the least charge transfer resistance in both electrodes. This result indicates that the di-membrane BPM must be operated under humidified conditions, due to the addition of the AEM layer causing a decrease in total current output compared to hybrid devices using only a Nafion membrane. Additionally, it is noteworthy that the despite the current/voltage profiles looking extremely similar (Figures 4 and 5), there are significant differences in the impedance spectra. The cell with only the cathode humidified shows the largest resistance in all three calculated components (interfacial, anode, and cathode). The most plausible explanation is that a larger amount of water was being drawn from the saturated cathodic feed and diffusing through the entire cell to hydrate the anode. The large resistance observed is then a result of measuring the high resistance of water transport, as opposed to the fully humidified cell wherein each electrode is hydrated slightly by its own gas feed. In the fully humidified cell, less water should be absorbed by each electrode from its feed stream, resulting in less overall mass transport of water throughout the device.

Table II. Computed circuit elements from EIS data.

Element	Epoxy	[bmim][OH]	Nafion
R_{mem} Ω cm^2	4.8	1.3	2.4
$R_{a,\,ct}$ Ω cm^2	3.6	8.4	7.9
$R_{c,ct}$ Ω cm^2	5.8	5.0	1.8

The di-membrane BPMs with conductive junction regions were also tested under fully humidified conditions. The Nyquist plots at ∼28 mA for those devices are shown in Figure 8, with the computed circuit elements tabulated in Table II.

From the data in Table II, both of the conductive interfaces displayed lower total high-frequency resistance (R_{mem} as labeled) than the neutral, epoxy junction. The epoxy-based MEA had the highest overall membrane resistance due to the negligible conductivity as a result of having both anionic and cationic species present to neutralize each other. For the [bmim][OH] and Nafion junction cells, it can be seen that using a [bmim][OH] hydroxide conductive material results in a lower overall membrane series resistance. When using the [bmim][OH] hydroxide conductive material, the water forms (proton-hydroxide recombination) on the PEM side of the PEM/AEM interface, which is farther from the AEM electrode than in the case of Nafion junction. The location of the [bmim][OH] junction appears the

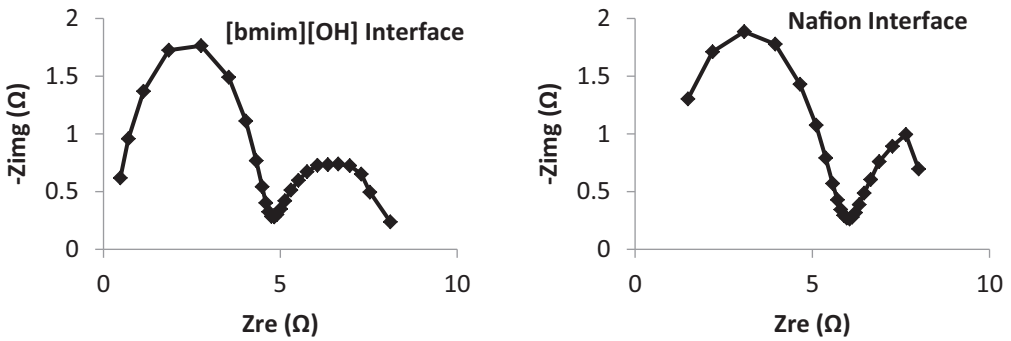

Figure 8. Nyquist plots for the MEAs with varying interfacial materials at 100% RH.

Table III. Summary of junction location and membrane resistance results at equivalent current.

	Epoxy	[bmim][OH]	Nafion
Conductive species	0 net	OH^-	H^+
Water formation location	Anywhere in junction	PEM side of junction	AEM side of junction
Membrane resistance (Ω cm^2)	4.8	1.3	2.4

determining factor giving the [bmim][OH] better device performance. A summary of these results is in Table III.

The junction location also appears to be a more prominent factor in determining the membrane resistance than the magnitude of the conductivity of the interfacial material. The conductivity of the ionic liquid [bmim][OH] junction is expected to be less than that of the Nafion ionomer dispersion[9] junction. Although the ionic liquid has lower conductivity than the Nafion ionomer junction, the lower high-frequency resistance shows a superior interfacial structure. However, this effect could also be due to the differing compositions of the interfacial solutions used. The [bmim][OH] ionic liquid was 10% v/v, while the Nafion dispersion is only 5%. Additionally, the lower interfacial resistance could also be a result of the water being formed as close to the middle of the cell as possible, due to Nafion 117 being appreciably thicker than A201 ($\sim$170 vs $\sim$30 μm).

In addition to changing the membrane resistance, moving the junction location also affected resistance in the electrode layers. The device using the neutral, epoxy-based junction showed lower charge transfer resistance in the anode than the cathode, while the devices using conductive interfaces exhibited the opposite. The most extreme case is the low cathodic resistance for the device using the Nafion dispersion interface, in which water forms on the AEM side of the junction region. Because the water is forming very near to the cathode, that electrode now has two water sources: the water formed at the junction and the humidified feed stream. With two such water sources, it is likely that there is very little mass transport of water through the cathode electrode layer.

The last point of interest concerns the impedance data. It was used to generate the Nyquist plots and tables discussed above. The data was collected at the same current, approximately 28 mA. For the devices using the epoxy and Nafion interfaces, the data was collected at 300 mV – relatively large overpotentials. For the device using the [bmim][OH] interface, the 28 mA current corresponded to a cell potential of 600 mV. The comparisons were done using the same current in order to ensure that the rate of water generation would be the same for each data set, since the water formation rate is directly proportional to the current. However, because of the cell voltage discrepancy between the devices, the overall performance of the device with the [bmim][OH] interface far exceeded that of the other interfaces. The voltammogram for this device is shown below in Figure 9.

The lower total interfacial resistance led to this device greatly outperforming the other samples. At an equivalent cell voltage (300 mV) to the other analyses above, both the interfacial and charge transfer resistances are heavily reduced in comparison to the other interfaces, as shown in Table IV.

The lower charge transfer resistance is expected at higher current loads, but it is important to note that the interfacial resistance remained relatively similar, as the high frequency intercept should be a constant parameter since it is a function of the membranes' ionic resistance and any hardware contact resistances. However, because the device exhibited a much lower high frequency intercept than its counterparts, it was able to produce much greater current loads at higher overpotentials, resulting in the large decrease in charge transfer resistance in the electrode layers.

Mono-membrane BPM characterization.—Pristine Nafion in sulfonic acid (R-SO_3H) form was reacted with thionyl chloride at 80°C

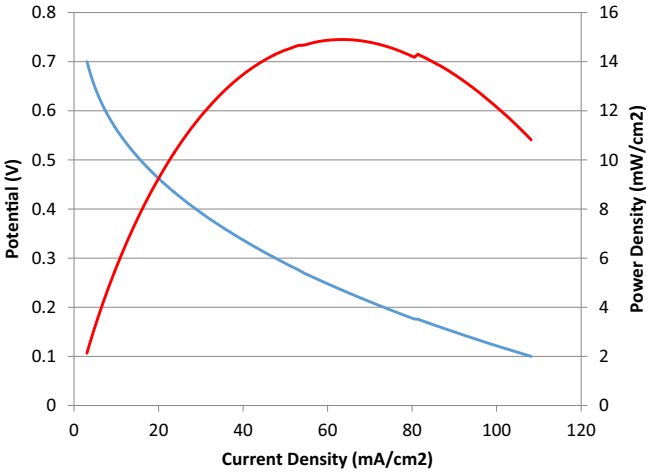

Figure 9. Voltammogram for the device with [bmim][OH] interface.

Table IV. Computed circuit elements for [bmim][OH] device at varying current output.

Element	95 mA (300 mV)	28 mA (600 mV)
R_{mem} Ω cm^2	1.6	1.3
$R_{a,\,ct}$ Ω cm^2	1.1	8.4
$R_{c,ct}$ Ω cm^2	0.9	5.0

for 12 hours to exchange the hydroxyl substituent for chloride. The hydroxyl portion of the sulfonic acid group is used for the ionic conduction of protons in standard PEM device operation. There is no known reaction at this time for directly converting this acidic site into any aminated form, hence the choice of the sulfonyl halide intermediate. The degree of chlorination on the reacted surface of the Nafion was determined using XPS. Table V shows the atomic composition of the surface which was exposed to thionyl chloride.

From Table V, the degree of chlorination on the surface can be computed by taking the ratio of chlorine to sulfur (i.e. at 100% conversion, the Cl/S ratio would be 1), since there can at most be 1 chlorine atom per sulfonic acid group. The surface conversion achieved here is 78%.

SIMS was employed to determine the depth of the chloride concentration in the sample. The counts of chloride were tracked with penetration depth into the sample. Although there are many possible heavy fragments that could have contained the chloride of interest (i.e. SO_2Cl and any cleavage of the side chain), these are difficult to track due to many other similarly heavy mass fragments possibly being produced via breakage of the polymer backbone and side chains. For this reason, it was determined that Cl^- (mass 35.5) was the only viable charged species that could be uniquely identified to contain any chlorine. Figure 10 shows the normalized depth profile of chloride ions in the film, revealing that the degree of chlorination reaches $\sim$10% of the surface after just 5 μm. After this 5 μm depth, the counts are low enough that they are considered residual signal.

After determining the depth of halogenation, the sample was aminated and quaternized as described previously, then re-examined using

Table V. Surface composition obtained from XPS.

Element	Atomic %
F	30.76
C	56.84
O	8.56
Cl	1.68
S	2.16

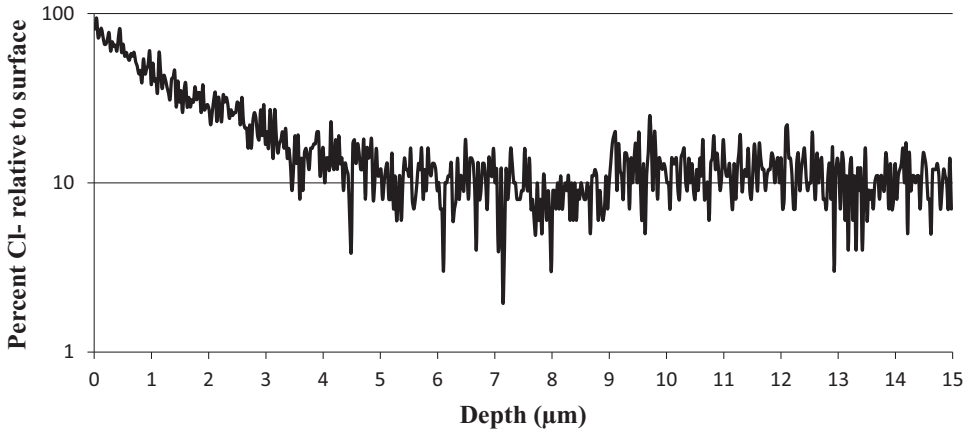

Figure 10. Depth profile of chloride ions, normalized to initial surface concentration.

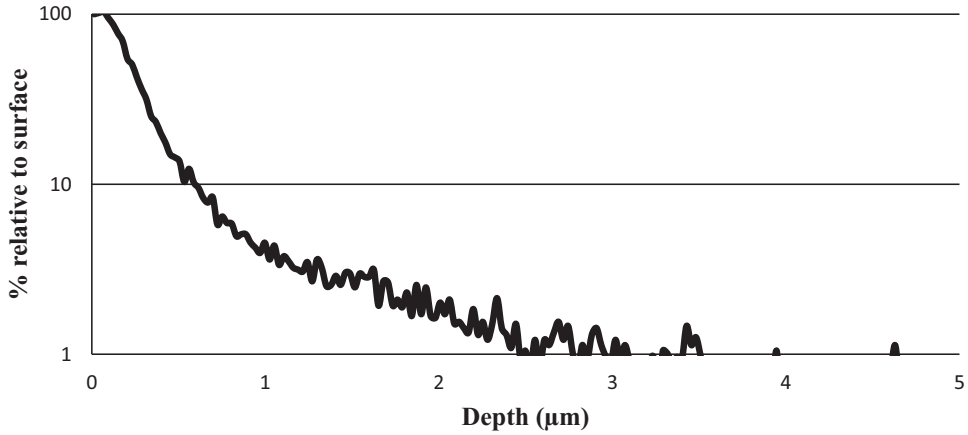

Figure 11. Normalized depth profile of cationic markers showing addition of amine chain.

SIMS to determine the depth of conversion to ammonium groups. For the quaternized sample, cationic markers were used, rather than the anionic chloride marker used for the halogenated film. This choice is due to the large M/Z ratio for iodide being nearly impossible to distinguish from polymeric chain fragments. This led to the choosing of $C_2H_4^+$, CH_2N^+, and $C_2H_6N^+$ as easily identifiable markers that could only be produced from the amine chain introduced via the amination and quaternization reactions. Figure 11 shows the depth profile normalized for the total concentration of the aforementioned markers.

The depth profile following quaternization shows that the depth of the AEM region only extends ~3 μm into the surface of the original Nafion film. Combining this result with the depth profile from the halogenated sample indicates that the top 3 μm is anionically conductive, the next 2 μm is still in the sulfonyl chloride state, and the remainder of the film is still in its default proton conductive form.

This mono-membrane BPM was incorporated into a working MEA similar to the devices constructed using the two-membrane BPMs. Unfortunately, the cell failed to produce appreciable current to record further measurements. Two possible reasons have been considered for this device failure: the most likely explanation is the enormously large width (~2 μm) of the neutral region relative to the desired junction, which is 3 orders of magnitude narrower (per the computational supplement to this work done in Ref. 6), resulting in excessive resistance over the interfacial region. Another possible reason is thermal stressing of Nafion due to repeated application of one face to a dry, heated surface.

Conclusions

Di-membrane bipolar membrane fuel cells with different interfacial materials were fabricated and characterized via EIS. The junction materials chosen were neutral, anion conductive, and proton conductive. Each material results in a different specific location of the PEM/AEM junction in the bipolar device, depending on the polarity of its conductivity. It was found that the location of the junction is a greater contributing factor than the conductivity of the interfacial material. From these experiments, the formation of the PEM/AEM junction on the surface of the PEM results in the lowest overall membrane resistance and highest total current output, an improvement greater than an order of magnitude over the initial work on bipolar devices.

Additionally, a mono-membrane BPM was fabricated via the conversion of a single face of Nafion. Although this membrane failed to perform during MEA testing, refining the synthetic scheme to more closely control penetration depths should allow for a BPM with significantly reduced ionic resistance, as compared to a di-membrane BPM. Another possible approach for improvement is exploration of newly developed electrospun BPMs,[10] which could more rigorously control the depths of the three regions in the BPM (PEM, junction, and AEM) since each portion is individually fabricated atop the others. Utilizing these improvements should continue to push to performance of BPM-based devices ever higher, as junction location control becomes more refined.

Acknowledgments

Financial support from US Office of the Deputy Assistant Secretary of the Army for Defense Exports and Cooperation (DASA-DE&C) is gratefully acknowledged. The authors would also like to thank Jared Schwartz and Oluwadamilola Phillips for their time and assistance performing the SIMS and XPS characterizations.

References

1. A. Schulze and E. Gulzow, *Journal of Power Sources*, **127**(1–2), 252 (2004).
2. K. Matsuoka, Y. Iriyama, T. Abe, M. Matsuoka, and Z. Ogumi, *Journal of Power Sources*, **150**, 27 (2005).
3. J. R. Varcoe, R. C. T. Slade, G. L. Wright, and Y. L. Chen, *Journal of Physical Chemistry B*, **110**(42), 21041 (2006).
4. M. Unlu, J. F. Zhou, and P. A. Kohl, *Journal of Physical Chemistry C*, **113**(26), 11416 (2009).
5. J. F. Zhou, K. Joseph, J. M. Ahlfield, D. Y. Park, and P. A. Kohl, *Journal of the Electrochemical Society*, **160**(6), F573 (2013).
6. K. N. Grew, J. P. McClure, D. Chu, P. A. Kohl, and J. M. Ahlfield, *Journal of the Electrochemical Society*, **163**, F1572 (2016).
7. M. Unlu, J. F. Zhou, and P. A. Kohl, *Journal of the Electrochemical Society*, **157**(10), B1391 (2010).
8. J. Zhou, J. S. Guo, D. Chu, and R. R. Chen, *Journal of Power Sources*, **219**, 272 (2012).
9. E. B. Fox, H. R. Colon-Mercado, Y. X. Chen, and W. S. W. Ho, *Ionic Liquids: Science and Applications*, **1117**, 129 (2012).
10. C. Shen, R. Wycisk, and P. N. Pintauro, *Energy and Environmental Science*, **10**, 1435 (2017).